Supporting Information

Observation of Selective Plasmon-Exciton Coupling in Nonradiative Energy Transfer: Donor-Selective *vs*. Acceptor-Selective Plexcitons

Tuncay Ozel, [§,γ] *Pedro Ludwig Hernandez-Martinez,* [†, ‡,§, γ] *Evren Mutlugun,* [†, ‡,§] *Onur Akin,* [§] *Sedat Nizamoglu,* [§] *Ilkem Ozge Ozel,* [§] *Qing Zhang,* [‡] *Qihua Xiong,* [‡, *] *and Hilmi Volkan Demir,* [†, ‡,§,*]

[†] Nanyang Technological University, *LUMINOUS!* Center of Excellence for Semiconductor Lighting and Displays, School of Electrical and Electronic Engineering, Singapore 639798

[‡] Nanyang Technological University,School of Physical and Mathematical Sciences, 21 Nanyang Link, Singapore 637371

[§] Bilkent University, Department of Physics, Department of Electrical and Electronics Engineering, and UNAM – Institute of Materials Science and Nanotechnology, TR-06800, Ankara, Turkey

[γ] These authors contributed equally to this work.

[*] To whom correspondence should be addressed. E-mail: hvdemir@ntu.edu.sg, Qihua@ntu.edu.sg, volkan@stanfordalumni.org

Theoretical Model

In this section we present a theoretical approach to the problem of selectively plasmon coupled nonradiative energy transfer pairs of colloidal quantum dots. The goal is to describe the optical properties of a complex structure composed of metal nanoparticles (MNPs) and semiconductor quantum dots (QDs). The main resulting interactions are exciton-exciton and exciton-plasmon interactions. For this reason, we separate our problem into four cases: 1) Plasmon enhanced QDs; 2) Förster-type Nonradiative energy transfer (FRET) in QDs pair; 3) Plasmon enhanced donor QDs and FRET in QDs pair; and 4) Plasmon enhanced acceptor QD and FRET in QDs pair. The following subsections describe each particular case.

Plasmon Enhanced QDs

Here, we present a description for the optical properties of a complex structure composed of a single QD and a single MNP under exciton-plasmon interaction. We consider a single QD interacting with a MNP in the presence of a constant electric field (see Figure 1). Within the simplest rate model, the number of excitons (N_{exc}) trapped in the QD, under constant illumination (steady-state condition), is given by

$$-(\gamma_r + \gamma_{nr} + \gamma_{nr,metal})N_{exc} + I_{abs} = 0 \qquad \text{Eq. 1}$$

where I_{abs} is the intensity of light absorption in the QD, $\gamma_{r(nr)}$ is the QD radiative (nonradiative) rate, and $\gamma_{nr,metal}$ is the exciton recombination rate of the QD because of energy transfer to the MNP. $\gamma_{nr,metal}$ is calculated by[1]

$$\gamma_{nr,metal} = \frac{2}{\hbar} b_\alpha \left(\frac{ed_{exc}}{\varepsilon_{eff}} \right)^2 \frac{R_{MNP}^3}{d^6} \left| \frac{3\varepsilon_0}{2\varepsilon_0 + \varepsilon_{MNP}(\omega)} \right|^2 \mathrm{Im}\left[\varepsilon_{MNP}(\omega)\right] \quad \text{Eq. 2}$$

where $b_\alpha = \frac{1}{3}.\frac{1}{3},\frac{4}{3}$ for $\alpha = x, y, z$ respectively, ε_0 is the dielectric constant of the outside medium, $\varepsilon_{MNP}(\omega)$ is the dielectric function of the MNP, R_{MNP} is the MNP radius, ed_{exc} is the exciton dipole moment in the QD, d is the center-to-center separation distance between the QD and MNP, and ε_{eff} is the effective dielectric constant given by

$$\varepsilon_{eff} = \frac{2\varepsilon_0 + \varepsilon_{SQD}}{3} \quad \text{Eq. 3}$$

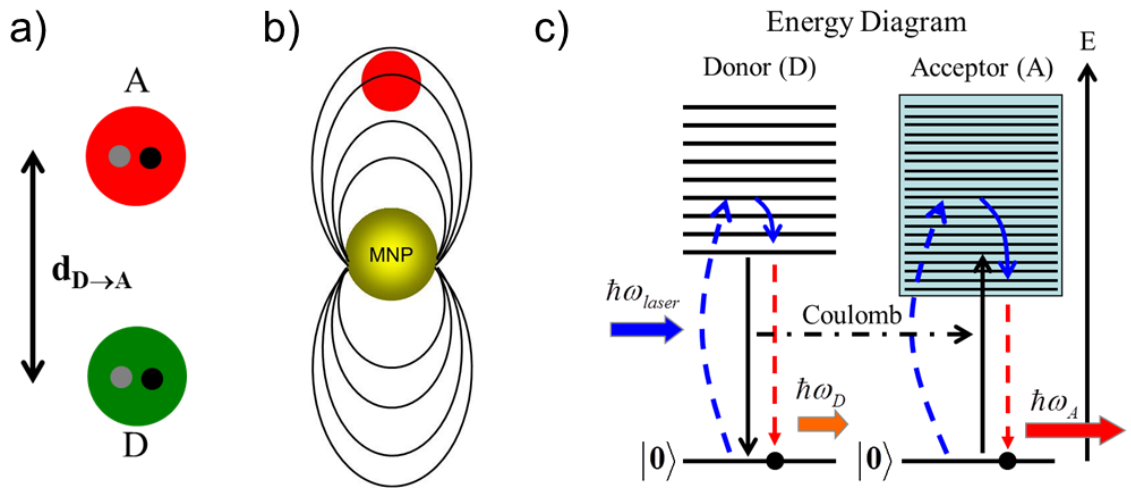

Figure 1. a) Donor-Acceptor (D-A) schematic for single donor (D) and acceptor (A). b) Plasmon enhances QD. c) Energy diagram for the D-A pair energy transfer process. Blue dash lines represent the absorption process of the nanostructure (donor/acceptor). Blue solid lines show fast relaxation process. Red dash lines show light emission process (relaxation from the lowest excited state to ground state). Black solid lines represent the energy transfer

from the donor to the acceptor. Horizontal solid black line shows the Coulomb interaction between the donor and acceptor(energy diagram is adapted from our previous publication[4]).

Here, we assume that the nonradiative rate is not affected by the MNP $\left(\gamma_{nr} = \gamma_{0,nr}\right)$, whereas the radiative rate and the absorption intensity are modified by the MNP. We make this assumption because the experiment is set up to enhance the emission of the QD in the presence of MNP. The absorption and radiative rate are modified by[2]:

$$I_{abs} = A(\omega_{laser}) I_{0,abs} \qquad \text{Eq. 4}$$

$$\gamma_r = A(\omega_{emiss}) \gamma_{0,r} \qquad \text{Eq. 5}$$

where $I_{0,abs}, \gamma_{0,r}, \gamma_{0,nr}$ are the parameters in the absence of MNP; $\omega_{emiss}(\omega_{laser})$ are the exciton-emission (excitation laser) frequencies; and $A(\omega)$ is the electric field enhancement factor defined as

$$A(\omega) = \frac{\int_{SQD} \left|E_{in,QD}\right|^2 dV}{\int_{SQD} \left|E_0\right|^2 dV} \qquad \text{Eq. 6}$$

where $E_{in,QD}$ is the electric field inside the QDs due to the presence of MNPs and E_0 is the electric field inside the QDs in the absence of MNPs. The integration is over the QD volume *V*. The emission intensity is written as

$$I_{emiss}(\omega)=\gamma_r N_{exc} F(\omega-\omega_{exc})=\frac{A(\omega_{emiss})\gamma_{0,r} A(\omega_{laser}) I_{0,abs}}{A(\omega_{emiss})\gamma_{0,r}+\gamma_{0,nr}+\gamma_{nr,metal}} F(\omega-\omega_{exc}) \quad \text{Eq. 7}$$

where $F(\omega)=a*\exp\left(-\frac{\omega^2}{2\sigma}\right)$ is a Gaussian function for the emission intensity distribution and a is a constant which depends on the unit system. Then, the emission enhancement factor $(\kappa_{PM}(\omega))$ for the SQD in the presence of MNP is

$$\kappa_{PM}(\omega_{emiss},\omega_{laser})=\frac{I_{emiss}(\omega)}{I_{0,emiss}(\omega)}=\frac{A(\omega_{emiss})A(\omega_{laser})\gamma_{0,exc}}{A(\omega_{emiss})Y_0\gamma_{0,exc}+(1-Y_0)\gamma_{0,exc}+\gamma_{nr,metal}} \quad \text{Eq. 8}$$

where $I_{0,emiss}(\omega)=Y_0 I_{0,abs} F(\omega-\omega_{exc})$ is the emission intensity in the absence of MNP. With $\gamma_{0,r}=Y_0\gamma_{0,exc}$, $\gamma_{0,nr}=(1-Y_0)\gamma_{0,exc}$. $\gamma_{0,exc}$ is the exciton recombination rate in the absence of MNP and Y_0 is the quantum yield for the QD.

FRET in QDs Pairs

Now, we proceed to estimate the FRET rate for D-A QD pair (Figure 1). Under the steady-state condition, the number of exciton in donor (acceptor) $N_{D,exc}(N_{A,exc})$ is given by the rate equations

$$-(\gamma_{D,r}+\gamma_{D,nr}+\gamma_{NRET})N_{D,exc}+I_{D,abs}=0 \quad \text{Eq. 9}$$

$$-(\gamma_{A,r}+\gamma_{A,nr})N_{A,exc}+\gamma_{NRET}N_{D,exc}+I_{A,abs}=0 \quad \text{Eq. 10}$$

Where $\gamma_{D,r}(\gamma_{A,r})$ is the donor (acceptor) radiative rate, $\gamma_{D,nr}(\gamma_{A,nr})$ is the donor (acceptor) nonradiative rate, and $I_{D,abs}(I_{A,abs})$ is the intensity of light absorption in the donor (acceptor). The D-A interaction is Förster-type given by

$$\gamma_{NRET} = \gamma_{D,exc}\left(\frac{R_0}{r}\right)^6 \quad \text{Eq. 11}$$

Here, R_0 is the Förster radius[3], $\gamma_{D,exc}$ is the exciton recombination rate of the D, and r is the separation distance between D and A. Then, the emission intensity for the donor (acceptor) is

$$I_{D,emiss}(\omega) = \gamma_{D,r} N_{D,exc} F(\omega - \omega_{D,exc}) = \frac{\gamma_{D,exc}}{\gamma_{D,exc} + \gamma_{NRET}} I_{0,D,emiss} \quad \text{Eq. 12}$$

$$I_{A,emiss}(\omega) = \gamma_{A,r} N_{A,exc} F(\omega - \omega_{A,exc}) = \left(1 + \frac{\gamma_{NRET}}{\gamma_{D,exc} + \gamma_{NRET}} \frac{I_{0,D,abs}}{I_{0,A,abs}}\right) I_{0,A,emiss} \quad \text{Eq. 13}$$

and the respective emission enhancement factors are $\left(I_{0,D,abs} \approx I_{0,A,abs}\right)$

$$\kappa_{D,NRET} = \frac{I_{D,emiss}(\omega)}{I_{0,D,emiss}(\omega)} = \frac{\gamma_{D,exc}}{\gamma_{D,exc} + \gamma_{NRET}} \quad \text{Eq. 14}$$

$$\kappa_{A,NRET} = \frac{I_{A,emiss}(\omega)}{I_{0,A,emiss}(\omega)} = 1 + \frac{\gamma_{A,exc}}{\gamma_{A,exc} + \gamma_{NRET}} \quad \text{Eq. 15}$$

Plasmon Enhanced Donor QD and FRET in QDs Pair

In this regard, we calculate FRET for the case of D-A QD pair in the presence of MNP coupled only to the donor QD (Figure 2) and estimate the emission intensity for the donor and acceptor QD. One, start with the rate equation for the donor and acceptor under the steady-state condition

$$-\left(\gamma_{D,r}+\gamma_{D,nr}+\gamma_{D,nr,met}+\gamma_{DPM\_NRET}\right)N_{D,exc}+I_{D,abs}=0 \quad \text{Eq. 16}$$

$$-\left(\gamma_{A,r}+\gamma_{A,nr}\right)N_{A,exc}+\gamma_{DPM\_NRET}N_{D,exc}+I_{A,abs}=0 \quad \text{Eq. 17}$$

where $N_{D,exc}\left(N_{A,exc}\right)$ is the number of exciton in the donor (acceptor), $\gamma_{D,r}=A_D\left(\omega_{D,emiss}\right)\gamma_{0,D,r}$; $\gamma_{D,nr}=\gamma_{0,D,nr}$; $I_{D,abs}=A_D\left(\omega_{laser}\right)I_{0,D,abs}$ are the radiative rate, nonradiative rate and absorption intensity of the donor in the presence of MNP at the donor side, respectively. $A_D\left(\omega_{D,emiss}\right)$ is the electric field enhancement factor for the donor due to the presence of MNP at the donor side. $\gamma_{A,r}=\gamma_{0,A,r}$; $\gamma_{A,nr}=\gamma_{0,A,nr}$; $I_{A,abs}=I_{0,A,abs}$ are the radiative rate, nonradiative rate and absorption intensity of the acceptor in the presence of MNP at the donor side. The subscript "0" denotes the variables in the absence of MNP.

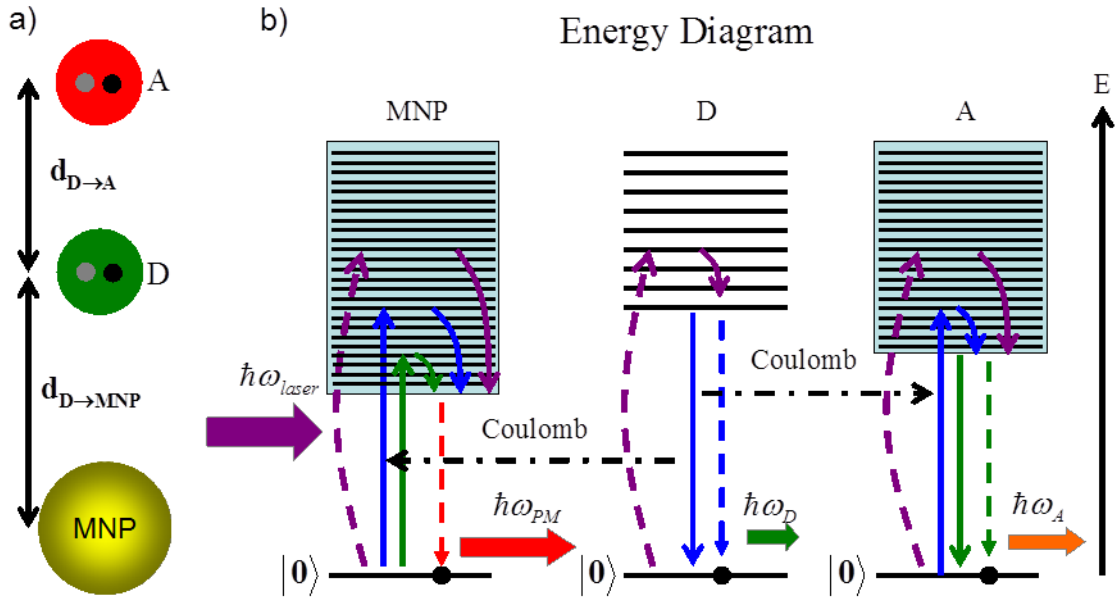

Figure 2. a) Donor-Acceptor (D-A) schematic for D-A pair when MNP is coupled only to donor QD. b) Energy diagram for the energy transfer process in the D-A pair when MNP is coupled only to donor QD. Purple dash lines represent the absorption process of the

nanostructure (MNP/donor/acceptor). Purple/blue solid lines show fast relaxation process. Red dash lines show light emission process (relaxation from the lowest excited state to ground state). Blue solid lines represent the energy transfer from the donor to the acceptor (QD/MNP). Horizontal dash black line shows the Coulomb interaction between the donor and acceptor(energy diagram is adapted from our previous publication[4]).

$\gamma_{D,nr,metal}$ is the exciton recombination rate of the donor QD because of energy transfer to the MNP couple to only donor.

$$\gamma_{D,nr,metal} = \frac{2}{\hbar} b_\alpha \left(\frac{ed_{D,exc}}{\varepsilon_{D,eff}} \right)^2 \frac{R_{MNP}^3}{d^6} \left| \frac{3\varepsilon_0}{2\varepsilon_0 + \varepsilon_{MNP}(\omega)} \right|^2 \mathrm{Im}\left|\varepsilon_{MNP}(\omega)\right| \quad \text{Eq. 18}$$

where $b_\alpha = \frac{1}{3}, \frac{1}{3}, \frac{4}{3}$ for $\alpha = x, y, z$ respectively, ε_0 is the dielectric constant of the outside medium, $\varepsilon_{MNP}(\omega)$ is the dielectric function of the MNP, R_{MNP} is the MNP radius, $ed_{D,exc}$ is the exciton dipole moment in the donor QD, d is the center-to-center separation distance between the donor QD and MNP, and $\varepsilon_{D,eff}$ is the donor effective dielectric constant given by

$$\varepsilon_{D,eff} = \frac{2\varepsilon_0 + \varepsilon_{D,SQD}}{3} \quad \text{Eq. 19}$$

And, $\gamma_{DPMNRET} = \gamma_{NRET}$ is the FRET between D-A QD pair. γ_{NRET} is given by Eq. 11. Thus, the donor (acceptor) emission intensity, $I_{D,emiss}(\omega) = \gamma_{D,r} N_{D,exc} F(\omega - \omega_{D,exc})$ $\left(I_{A,emiss}(\omega) = \gamma_{A,r} N_{A,exc} F(\omega - \omega_{A,exc})\right)$, is

$$I_{D,emiss}(\omega) = \kappa_{D,DPMNRET} I_{0,D,emiss}(\omega) \quad \text{Eq. 20}$$

$$I_{A,emiss}(\omega) = \frac{A_{AD}(\omega_{A,emiss}) A_{AD}(\omega_{laser}) \gamma_{0,D,exc}}{A_{AD}(\omega_{D,emiss}) Y_{0,A} \gamma_{0,A,exc} + (1-Y_{0,A}) \gamma_{0,A,exc} + \gamma_{A,nr,metal}} I_{0,A,emiss}(\omega)$$
$$\left(1 + \frac{\gamma_{NRET}}{A_D(\omega_{D,emiss}) Y_{0,D} \gamma_{0,D,exc} + (1-Y_{0,D}) \gamma_{0,D,exc} + \gamma_{D,nr,metal} + \gamma_{DPMNRET}} \frac{A_D(\omega_{laser})}{A_{AD}(\omega_{laser})} \frac{I_{0,D,emiss}(\omega)}{I_{0,A,emiss}(\omega)}\right)$$

Eq. 21

where $\kappa_{D,DPMNRET}$ is the donor emission enhancement factor when only the donor is coupled to MNP $I_{0,D,emiss}(\omega) \approx I_{0,A,emiss}(\omega)$.

$$\kappa_{D,DPMNRET} = \frac{A_D(\omega_{D,emiss}) A_D(\omega_{laser}) \gamma_{0,D,exc}}{A_D(\omega_{D,emiss}) Y_{0,D} \gamma_{0,D,exc} + (1-Y_{0,D}) \gamma_{0,D,exc} + \gamma_{D,nr,metal} + \gamma_{DPMNR}} \quad \text{Eq. 22}$$

$$\kappa_{A,DPMNRET} = \frac{A_{AD}(\omega_{A,emiss}) A_{AD}(\omega_{laser}) \gamma_{0,D,exc}}{A_{AD}(\omega_{D,emiss}) Y_{0,A} \gamma_{0,A,exc} + (1-Y_{0,A}) \gamma_{0,A,exc} + \gamma_{A,nr,metal}}$$
$$\left(1 + \frac{\gamma_{NRET}}{A_D(\omega_{D,emiss}) Y_{0,D} \gamma_{0,D,exc} + (1-Y_{0,D}) \gamma_{0,D,exc} + \gamma_{D,nr,metal} + \gamma_{DPMNRET}} \frac{A_D(\omega_{laser})}{A_{AD}(\omega_{laser})}\right) \quad \text{Eq. 23}$$

Plasmon Enhanced Acceptor QD and FRET in QDs Pair

Here, we calculate FRET for the case of D-A QD pair in the presence of MNP coupled only to the acceptor QD (Figure 3) and estimate the emission intensity for the donor and acceptor QD. Under the steady-state condition, the rate equations for the donor and acceptor are

$$-(\gamma_{D,r}+\gamma_{D,nr}+\gamma_{APM\_NRET})N_{D,exc}+I_{D,abs}=0 \quad \text{Eq. 24}$$

$$-(\gamma_{A,r}+\gamma_{A,nr}+\gamma_{A,nmet})N_{A,exc}+\gamma_{APM\_NRET}N_{D,exc}+I_{A,abs}=0 \quad \text{Eq. 25}$$

where $N_{D,exc}(N_{A,exc})$ is the number of exciton in the donor (acceptor), $\gamma_{D,r}=\gamma_{0,D,r}$; $\gamma_{D,nr}=\gamma_{0,D,nr}$; $I_{D,abs}=I_{0,D,abs}$ are the radiative rate, nonradiative rate and absorption intensity of the donor in the presence of MNP at the acceptor side respectively. $\gamma_{A,r}=A_A(\omega_{A,emiss})\gamma_{0,A,r}$; $\gamma_{A,nr}=\gamma_{0,A,nr}$; $I_{A,abs}=A_A(\omega_{laser})I_{0,A,abs}$ are the radiative rate, nonradiative rate and absorption intensity of the acceptor in the presence of MNP at the acceptor side. $A_A(\omega_{A,emiss})$is the electric field enhancement factor for the acceptor due to the presence of MNP at the acceptor side. The subscript "0" denotes the variables in the absence of MNP.

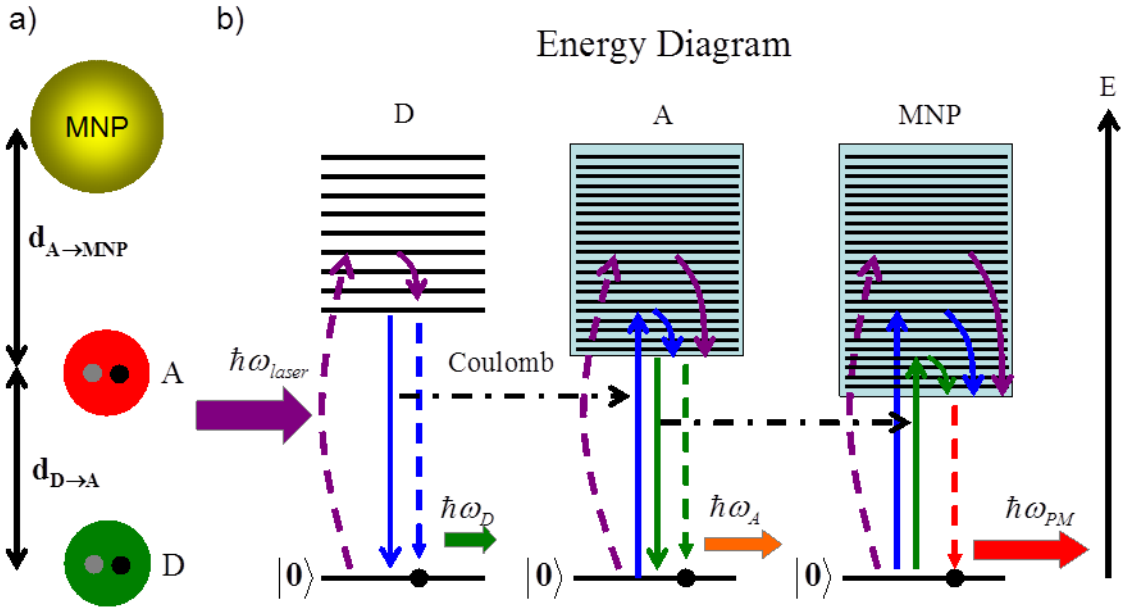

Figure 3. a) Donor-Acceptor (D-A) schematic for D-A pair when MNP is coupled only to acceptor QD. b) Energy diagram for the energy transfer process in the D-A pair when MNP is

coupled only to acceptor QD. Purple dash lines represent the absorption process of the nanostructure (MNP/donor/acceptor). Purple/blue solid lines show fast relaxation process. Red dash lines show light emission process (relaxation from the lowest excited state to ground state). Blue solid lines represent the energy transfer from the donor to the acceptor (QD/MNP). Horizontal dash black line shows the Coulomb interaction between the donor and acceptor(energy diagram is adapted from our previous publication[4]).

$\gamma_{A,nr,metal}$ is the exciton recombination rate of the acceptor QD because of energy transfer to the MNP coupled to only acceptor.

$$\gamma_{A,nr,metal} = \frac{2}{\hbar} b_\alpha \left(\frac{e d_{A,exc}}{\varepsilon_{A,eff}} \right)^2 \frac{R_{MNP}^3}{d^6} \left| \frac{3\varepsilon_0}{2\varepsilon_0 + \varepsilon_{MNP}(\omega)} \right|^2 \mathrm{Im}\left| \varepsilon_{MNP}(\omega) \right| \qquad \text{Eq. 26}$$

where $b_\alpha = \frac{1}{3}, \frac{1}{3}, \frac{4}{3}$ for $\alpha = x, y, z$ respectively, ε_0 is the dielectric constant of the outside medium, $\varepsilon_{MNP}(\omega)$ is the dielectric function of the MNP, R_{MNP} is the MNP radius, $ed_{A,exc}$ is the exciton dipole moment in the acceptor QD, d is the center-to-center separation distance between the acceptor QD and MNP, and $\varepsilon_{A,eff}$ is the acceptor effective dielectric constant given by

$$\varepsilon_{A,eff} = \frac{2\varepsilon_0 + \varepsilon_{A,SQD}}{3} \qquad \text{Eq. 27}$$

And, $\gamma_{APMNRET} = \gamma_{NRET}$ is the FRET between D-A QD pair. γ_{NRET} is given by Eq. 11. Thus, the donor (acceptor) emission intensity, $I_{D,emiss}(\omega) = \gamma_{D,r} N_{D,exc} F(\omega - \omega_{D,exc})$ $\left(I_{A,emiss}(\omega) = \gamma_{A,r} N_{A,exc} F(\omega - \omega_{A,exc}) \right)$, is

$$I_{D,emiss}(\omega) = \kappa_{D,APMNRET} I_{0,D,emiss}(\omega) \quad \text{Eq. 28}$$

$$I_{A,emiss}(\omega) = \kappa_{A,DPMNRET}\left(1 + \frac{\kappa_{A,DPMNRET}}{A_A(\omega_{laser})}\frac{\gamma_{NRET}}{\gamma_{0,D,exc}}\frac{I_{0,D,emiss}(\omega)}{I_{0,A,emiss}(\omega)}\right) I_{0,A,emiss}(\omega) \quad \text{Eq. 29}$$

where $\kappa_{D,APMNRET}$ is the donor emission enhancement factor when only the acceptor is couple to MNP (Eq. 30) and $\kappa_{A,APMNRET}$ is the acceptor emission enhancement factor when only the acceptor is coupled to MNP(Eq. 31) $I_{0,D,emiss}(\omega) \approx I_{0,A,emiss}(\omega)$.

$$\kappa_{D,APMNRET} = \frac{A_{DA}(\omega_{D,emiss}) A_{DA}(\omega_{laser}) \gamma_{0,D,exc}}{A_{DA}(\omega_{D,emiss}) Y_{0,D} \gamma_{0,D,exc} + (1 - Y_{0,D}) \gamma_{0,D,exc} + \gamma_{APMNRET}} \quad \text{Eq. 30}$$

$$\kappa_{A,DPMNRET} = \frac{A_A(\omega_{A,emiss}) A_A(\omega_{laser}) \gamma_{0,A,exc}}{A_A(\omega_{A,emiss}) Y_{0,A} \gamma_{0,A,exc} + (1 - Y_{0,A}) \gamma_{0,A,exc} + \gamma_{A,nr,meta}} \quad \text{Eq. 31}$$

Numerical Results

In this section we present our numerical results for the FRET for the four cases mentioned above. The parameters we used are: $R_{MNP} = 7.5\,nm$, $R_{DQD} = 1.8nm$, $R_{AQD} = 2.0nm$, $\lambda_{D,exc} = 590nm$, $\lambda_{A,exc} = 635nm$, $Y_{0,D} = 0.2$, $Y_{0,A} = 0.14$, $\tau_{0,D,exc} = 1.33\,ns$, $\tau_{0,A,exc} = 1.53ns$. We consider the dielectric constant for the outside media as

$$\varepsilon_m = \frac{\varepsilon_{PDDA} + \varepsilon_{PSS}}{2} \quad \text{Eq. 32}$$

Where $\varepsilon_{PDDA} = 2.0$ is the dielectric constant of the PDDA and $\varepsilon_{PSS} = 2.25$ is the dielectric constant of the PSS. Also, we consider that the thickness of the PDDA/PSS layer to be $1.1\,nm$. Figure 4 shows the emission enhancement for the QDs when either the donor or the

acceptor is coupled to the MNPs separately. From this figure, we observe an emission enhancement factor of 2.15 for the donor QDs and 2.31 for the acceptor QDs. These results are close to the experimental values of 2.25 and 2.69 for the donor and acceptor QDs respectively. Figure 5 depicts the FRET for the case of D-A QD pair. From here, we obtain an emission enhancement factor for the acceptor QDs of 1.46, which is comparable to the experimental value of 1.30. In addition, we observe quenching in the emission of the donor QDs. It reduces to 65% of its emission value

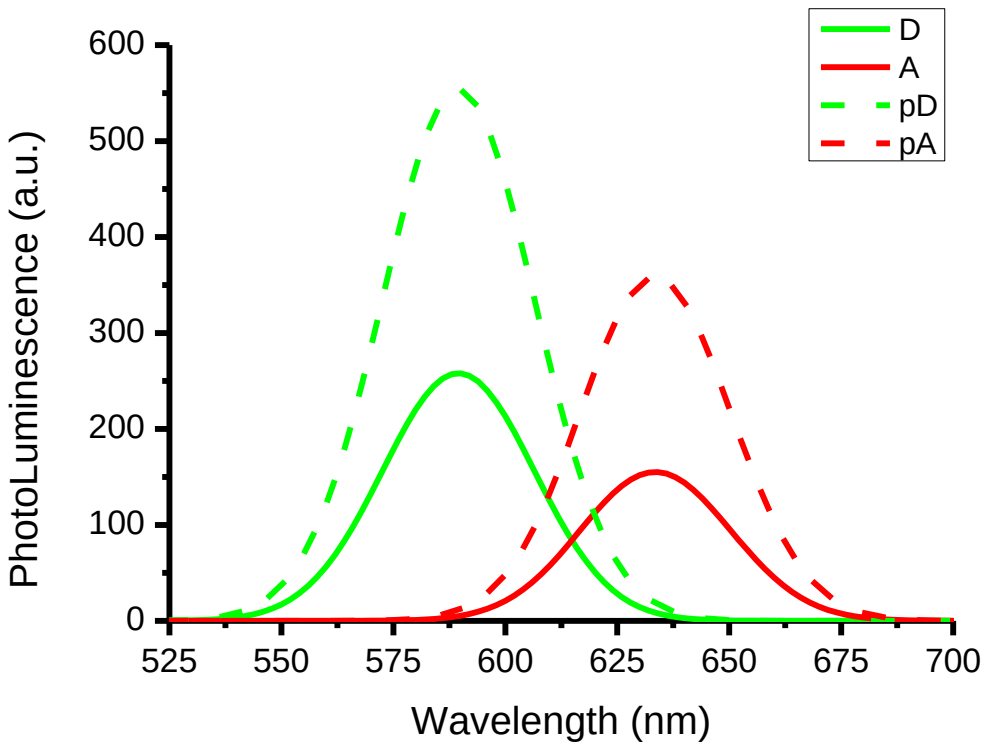

Figure 4: Photoluminescence for the donor (green color) and acceptor (red color) QDs. Solid line shows the QD emission in the absence of MNPs. Dash line illustrates the QD emission in the presence of MNP.

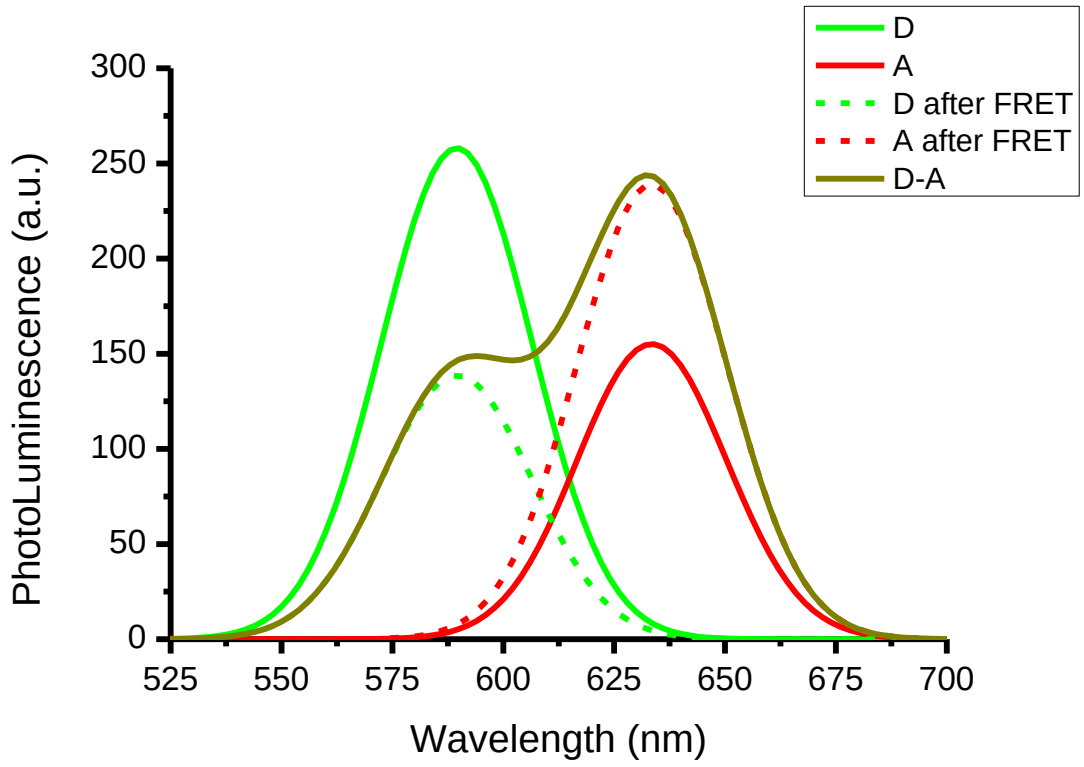

Figure 5: Photoluminescence (PL) for the D-A QD pair under the Förster-type energy transfer. Solid green line represents the donor emission before the D-A coupling. Solid red line illustrates the acceptor emission before the D-A coupling. Dark yellow line shows the PL intensity for the D-A QD. Green dash line shows the PL intensity of the donor after coupling with the acceptor. Red dash line illustrates the acceptor PL intensity after coupling with the donor.

Figure 6 illustrates the photoluminescence (PL) intensity for the D-A QD pair when MNP is coupled only to the donor QD. Here, we observe an increase on the PL intensity of 1.30 compare to the case without coupling to MNPs and acceptor QDs. This result is close to the

experimental value of 1.45. In the case of the acceptors we obtain an increase of the PL intensity of 2.80, which is comparable to the experimental value of 1.93. Figure 7 shows the PL intensity for the D-A QD pair when MNP is couple only to the acceptor QD. We observe a 26% decrease in the PL intensity of the donor. This quenching in PL intensity is due to the energy transfer between D and A QD. For the acceptor case, the PL intensity has increased 3.37 times. This result is comparable to the experimental value of 2.70 times.

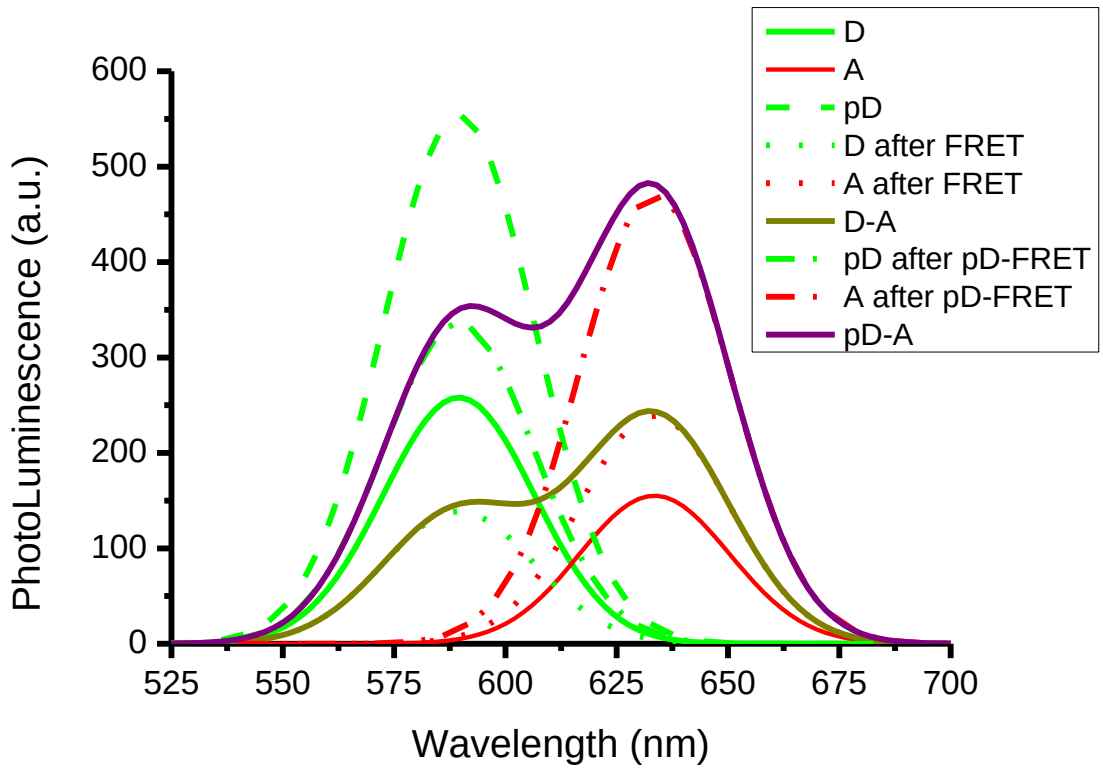

Figure 6: PL intensity for the D-A QD pair when MNP is coupled only to donor QD. Green (red) solid line represents donor (acceptor) PL intensity without coupling. Dash green line illustrates the PL intensity of the donor when it is coupled to only to MNP. Green and red dot line shows the PL intensity of the donor and acceptor when they are coupled to each other in the absence of MNP. Dark yellow solid line illustrates the FRET. Purple solid line shows the

FRET for the D-A QD pair when only the donor QD is coupled to MNP. Green (red) dash double dot line represents the PL intensity for the donor (acceptor) for this case.

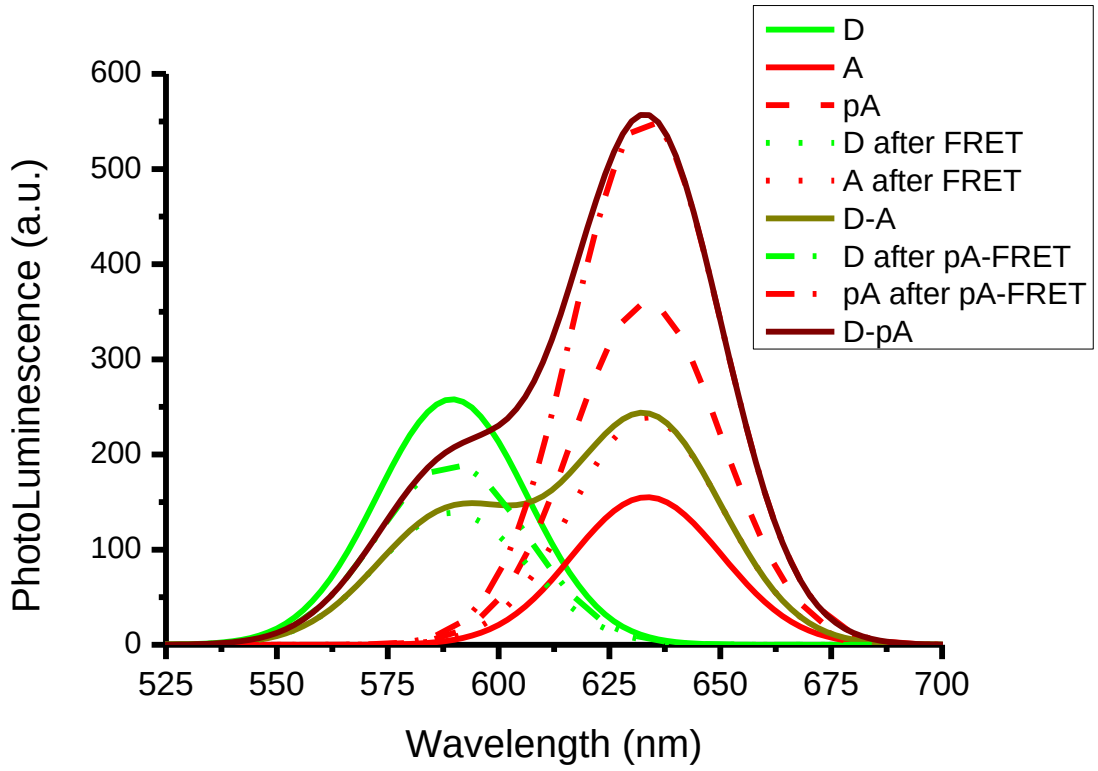

Figure 7: PL intensity for the D-A QD pair when MNP is coupled only to acceptor QD. Green (red) solid line represents donor (acceptor) PL intensity without coupling. Dash red line illustrates the PL intensity of the acceptor when it is coupled to only to MNP. Green and red dot line shows the PL intensity of the donor and acceptor when they are coupled to each other in the absence of MNP. Dark yellow solid line illustrates the FRET. Wine solid line shows the FRET for the D-A QD pair when only the acceptor QD is coupled to MNP. Green (red) small dot line represents the PL intensity for the donor (acceptor) for this case.

Experimental Characterization

Au MNP synthesis results in 15±2 nm nanoparticles as observed in transmission electron microscopy image depicted in Figure 8.

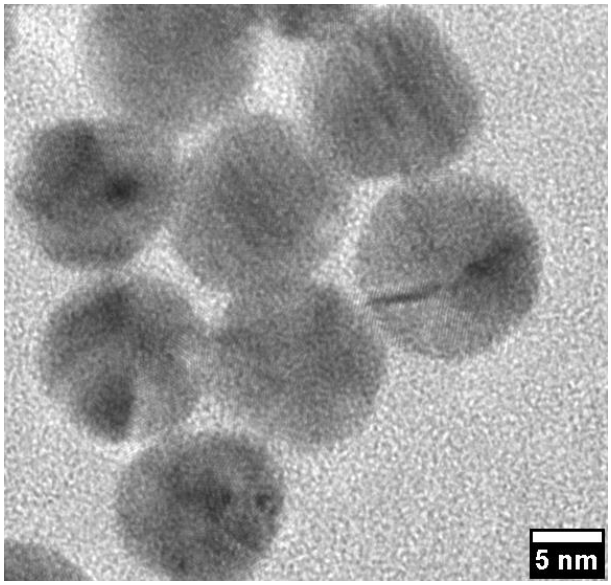

Figure 8. Transmission electron microscope image of synthesized Au nanoparticles.

In solution absorption spectrum of as synthesized Au nanoparticles show a plasmon resonance peak at 520 nm with a full width half maximum of 85 nm as depicted in Figure 9.

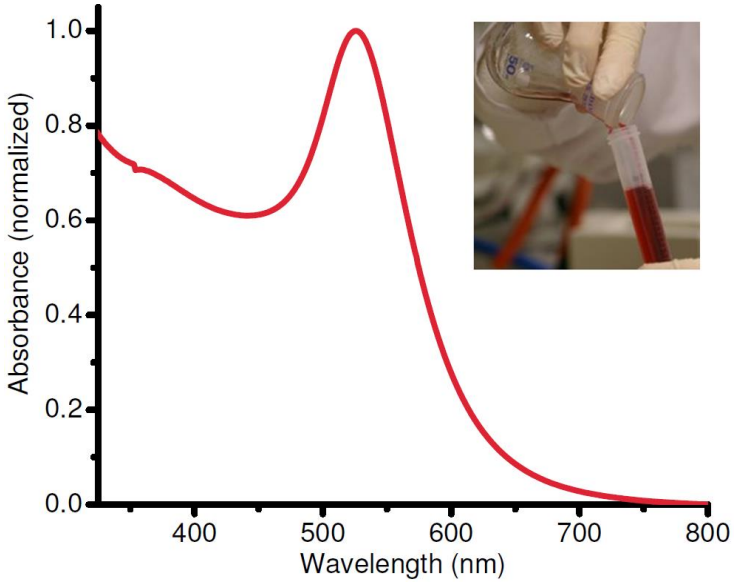

Figure 9. Normalized absorbance spectrum of colloidal Au nanoparticles. Inset is a picture of Au nanoparticles transferred into a vial after synthesis.

Quantum dots with various sizes, emitting at various wavelengths are synthesized by varying the reaction time during synthesis. A sample image of synthesized quantum dots emitting at different wavelengths are shown in Figure 10.

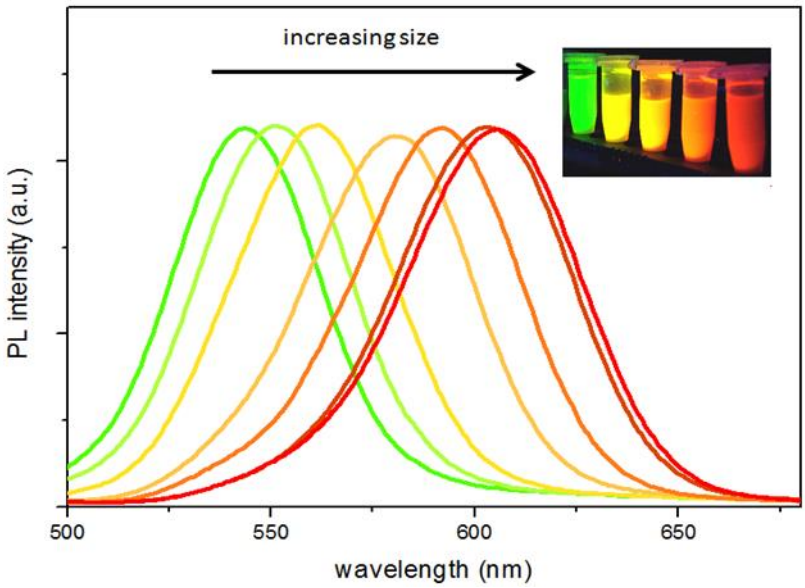

Figure 10. Photoluminescence spectra (normalized) of CdTe QDs emitting at various wavelengths depending on size controlled by increased reaction time during synthesis. Inset is a picture of CdTe QDs under UV light illumination (adapted from our previous publication[5]).

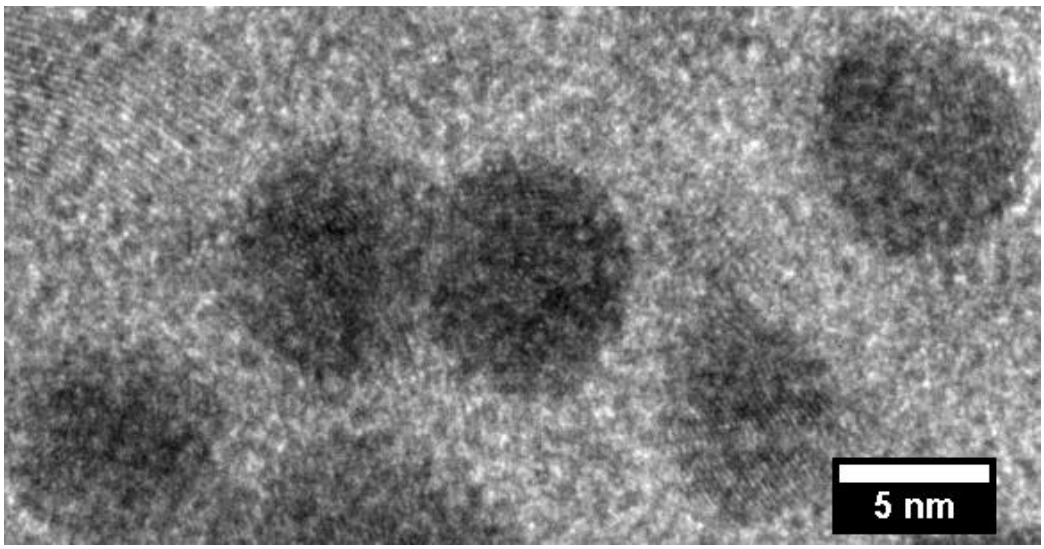

Figure 11. Transmission electron microscope image of synthesized CdTe QDs.

Layer-by-layer deposition of Au MNPs on Cu TEM grids show that Au MNPs stack on top of each other as number of layers are increased as depicted in Figure 12 and 13. Note that layer-by-layer deposition results in more homogenous distribution and stacking of particles on glass substrates (used in our experiments) compared to a TEM grid (used for imaging purposes) because of built-in negative charges on glass surface.

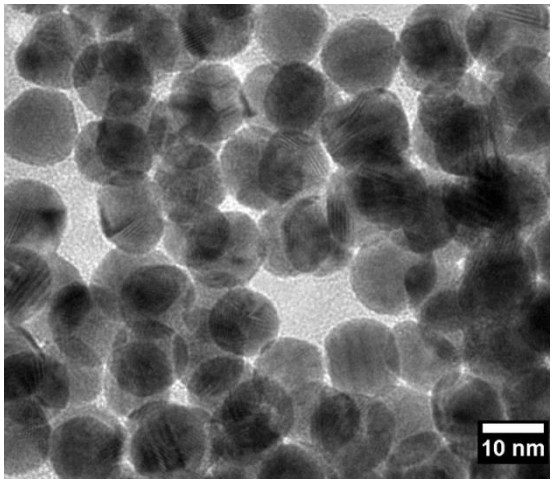

Figure 12. Transmission electron microscope image of one monolayer Au MNP coated TEM grid.

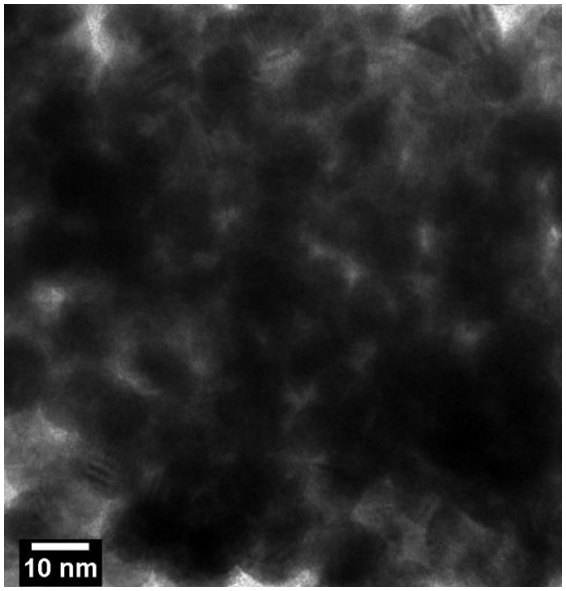

Figure 13. Transmission electron microscope image of a three monolayer Au MNP coated on TEM grid.

Layer-by-layer deposited one monolayer of CdTe QD is depicted in Figure 14. Surface coverage on TEM grid is lower compared to Au MNPs most likely due to lower electrostatic interaction between the surface of the grid and the surfactants of QDs. (Note that TEM grids are used only for imaging purposes, experiments are done on negatively charged glass substrates).

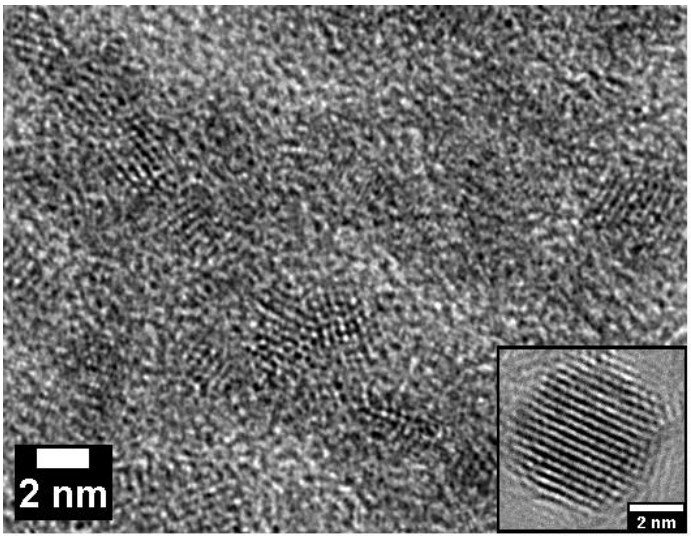

Figure 14. Transmission electron microscope image of one monolayer CdTe QD coated TEM grid. Inset is a high resolution zoomed in picture of a single CdTe QD.

The studied layer-by-layer assembled Au NP films make partially transparent films since the reflection (and also the extinction) values are actually not high. To confirm the transparency of our Au NP films, we prepared and deposited 6 MLs of Au NPs on a glass slide (with 4 MLs of PDDA/PSS in between them). As visual evidence, we placed this sample on the left side of a Nano Letters emblem printed on a white page. Looking from the top in plan view, as can be seen in Figure 15, the sample is highly transparent and the emblem is clearly visible through the Au nanoparticles, confirming that the reflection off the Au NPs from the top is not substantial under visible light illumination. Actually, we observe this reflection level to be very similar to that observed in the case of the starting substrate alone, mainly coming from the Fresnel reflection of the substrate itself. This observation also supports the fact that

this level of weak reflection is not sufficient to explain the emission enhancement levels obtained in our experiments and should not have any significant effect on the collected emission levels to favor the acceptor emission over the donor emission or vice versa.

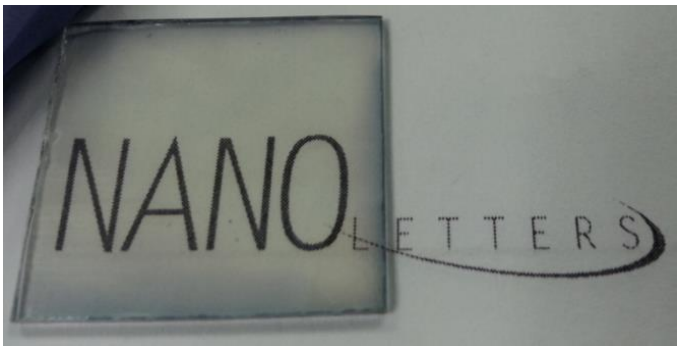

Figure 15. Picture of a Nano Letters emblem printed on a white paper completely visible through 6 MLs of Au NPs deposited on a glass substrate with no significant reflection off the Au NP film from the top under white light illumination.

Here it is also worth noting that the sample pictured in Figure 15 shows some typical variation in the resulting film towards the edges of its glass substrate, which is very common in samples prepared using layer-by-layer deposition, due to the edge effect. Except for the variation towards the edges, the resulting films are actually very clear and uniform. In our experiments, for this reason, the measurements have never been taken from these edges; all of our measurements have always been carried out using the middle part sufficiently far away the edge bead, which always gives nice, uniform and reproducible films.

To further quantify the reflection from the uniform part of the sample, we have also optically measured the reflection directly off the substrate in the middle before and after these 6 ML Au nanoparticles were assembled. This experimental data is presented in Table 1. As

expected, the starting reflection, which is ~20% for our operating wavelength range, comes from the Fresnel reflection due to the refractive index contrast between the glass and the air. With the Au nanoparticles deposition, the reflection slightly drops by a few percent (~15%) possibly due to a smoother surface with the use of polyelectrolytes and better impedance matching between the glass and the air. This basically allows maintaining essentially a similar level of reflection.

	Only Glass (% Reflection)	**Glass with Au NPs (% Reflection)**
@ Donor Wavelength (591 nm)	20.0	15.1
@ Acceptor Wavelength (635 nm)	20.5	15.9

Table 1. Reflection from the glass substrate with and without 6 MLs of Au NPs measured at the donor and acceptor emission wavelengths. The reflection measurements are done using a commercial micro-reflectance/transmission spectrometer (Craic 20/20 PVTM UV-Vis-NIR Dual Microspectrophotometer). White light source generated from the halogen lamp is focused onto the samples by a 15x reflective objective (NA: 0.28) with a normal incident to the sample. The reflected light is collected by the same objective and analyzed by a monochromator.

Also, it is important to emphasize that the emission enhancement levels obtained using the steady-state measurements are fully supported by the time-resolved emission kinetics data. As discussed in the manuscript, we presented the emission kinetics of the quantum dots

measured systematically using time-resolved fluorescence spectroscopy. This allowed us to obtain a family of photoluminescence decay curves and to clearly identify the lifetime modifications in the presence of coupled gold nanoparticles. Evidently, the lifetime of the donor QDs alone (and also true for the acceptor QD) was strongly modified when in the presence of proximal Au NP films. Unlike what is measured over and over in our experiments, the reflection of emitted photons from a surface cannot change their emission kinetics. Such lifetime modifications are therefore simply not possible with a mirror-like reflector effect alone. Thus, this means that there has to be a near-field effect coming from the coupling of the photogenerated excitons in the QDs with the proximal plasmonic film in the near field to modify the emission lifetimes of the QDs. Furthermore, the enhancement levels calculated using these measured lifetime modifications agree well with the actual enhancement levels obtained using the steady state far-field measurements. Since the far-field measurements, which could be in principle affected both from the near-field plasmonic coupling and the reflection, do not give us a significantly different enhancement than those calculations based on the lifetime modifications, which can come only from near-field plasmon coupling. In addition to the evidences discussed above, that is why we can deduce that the far-field reflection from such a thin Au NP film is small, so that the emission enhancement owing to the reflection was insignificantly small.

The sample, consisting of Au NP and QDs layer was cut into two pieces and the SEM image was taken along the cutting edges. Layer-by-layer nature of the composite film containing Au NP and QD layers is depicted in Figure 16. However, resolving monolayers of QDs and Au

NPs with a higher resolution is not possible due to electron beam charging in the presence of glass and dielectric polymers that were used in the layer-by-layer assembly process. Still, the total length of this layered section is measured to be ~129 nm. This sample contains 4 ML PDDA/PSS (~4.4 nm) + 6 ML Au NP (~90 nm + 3.6 nm PDDA) + 4 ML PDDA/PSS (~4.4 nm) + 1 ML donor QD (~4.5 nm + 0.6 nm PDDA) + 3 ML PDDA/PSS (~3.3 nm) + 1 ML acceptor QD (~5.1 nm + 0.6 nm PDDA). Using expected values given for each layer, this sample should have a total thickness of ~116.5 nm (including the thickness of PDDA layers used to deposit Au NPs and QDs, but excluding the thickness of the surfactants).

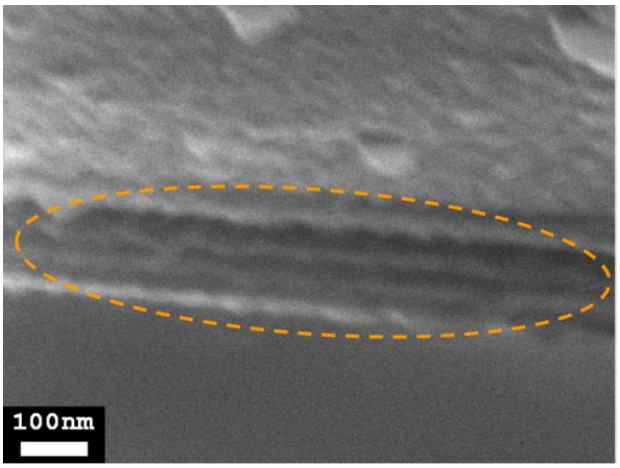

Figure 16. Cross-sectional SEM image of Au NP and QD layers deposited on a glass substrate (glass side in the bottom).

In our time-resolved experiments, samples are excited via a picosecond laser at 375 nm aligned in vertical polarization. A high precision vertical polarizer and high quality lens systems are used to focus laser beam onto top side of the substrate. Following the excitation, emitted light from the sample is passed through a UV filter (400 nm cut-off to eliminate collection of excitation source reflections from the substrate) and followed by a linear

polarizer at so-called magic angle (54.7^0 to eliminate emission anisotropy effects). Finally, photons passing through a monochromator at a specific wavelength (donor emission wavelength or acceptor emission wavelength) with 0.5 mm slits are counted via a high precision time-correlated single photon counting system (Picoquant-FluoTime200). Experimental setup is illustrated in Figure 17.

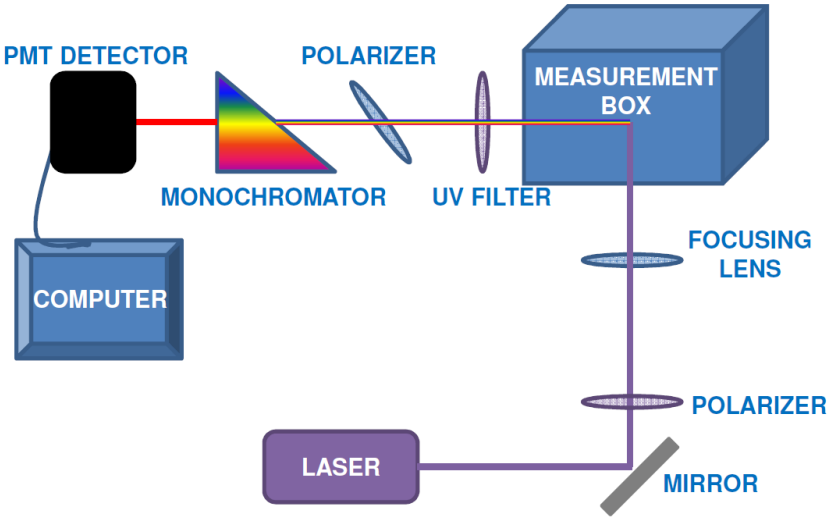

Figure 17. Illustration of the optical setup for time-resolved fluorescence measurements.

We analyzed the emission kinetics by calculating the decay lifetimes of QDs using commercially available multi-exponential decay fit analysis software (FluoFit, Picoquant GmbH, Germany). Function depicted in equation S1 is used by the software to fit the decay curves.

$$I(t) = \int_{-\infty}^{t} I\,RF(t') \sum_{i}^{n} A_i e^{-\frac{t-t'}{\tau_i}} dt' \qquad \text{Eq. 33}$$

Here, for an n-exponential decay fit parameters A_i stands for the amplitude and and τ_i stands for the decay lifetime of the i^{th} component. Instrument response function (abbreviated as IRF in the equation) is deconvoluted from the measured decay curve to eliminate excitation source-detector response related errors in decay analysis of the sample (via measuring the decay curve of sample at excitation wavelength with a scattering sample). Using the software package, we optimize the lifetime values to optimize the chi square, X^2value (with unity representing the best match), which shows the match between the measured curve and the fitted curve using 3-exponential model.

REFERENCES

1. Govorov, A.O.; Lee, J.;Kotov, N.A. *Phys. Rev. B***2007**, 76, 125308.
2. Govorov, A. O.; Bryant, G. W.; Zhang, W.; Skeini, T.; Lee, J.; Kotov, N. A.; Slocik, J. M.; Naik, R. R. *Nano Lett.***2006**, *6*, 984-994.
3. Lakowicz J.R.,"Principles of Fluorescence Spectroscopy" *3rd Edition*, Springer **2006**.
4. Mutlugun, E.; Hernandez-Martinez, P. L.; Eroglu, C.; Coskun, Y.; Erdem, T.; Sharma, V. K.; Unal, E.; Panda, S. K.; Hickey, S. G.; Gaponik, N.; Eychmüller, A.; Demir, H. V. *Nano Lett.***2012**, *12*, 3986-3993.
5. Ozel, T.; Nizamoglu, S.; Sefunc, M. A.; Samarskaya, O.; Ozel, I. O.; Mutlugun, E.; Lesnyak, V.; Gaponik, N.; Eychmuller, A.; Gaponenko, S. V. ; Demir, H. V. *ACS Nano***2011**, *5*, 1328-1334.